

Exploring multi-step electroweak phase transitions in the 2HDM+ a

Zong-guo Si¹, Hong-xin Wang¹, Lei Wang², and Yang Zhang^{3,4}

¹*School of Physics, Shandong University, Jinan, Shandong 250100, China*

²*Department of Physics, Yantai University, Yantai, Shandong 264005, China*

³*School of Physics, Zhengzhou University, Zhengzhou 450000, China*

⁴*School of Physics, Henan Normal University, Xinxiang 453007, China*

Abstract

Multiple electroweak phase transitions occurring sequentially in the early universe can give rise to intriguing phenomenology, compared to the typical single-step electroweak phase transition. In this work, we investigate this scenario within the framework of the two-Higgs-doublet model with a pseudoscalar, utilizing the complete one-loop finite-temperature effective potential. After considering relevant experimental and theoretical constraints, we identify four distinct types of phase transitions. In the first case, only the configuration of the CP-even Higgs acquires a non-zero value via a first-order or a cross-over electroweak phase transition, leading to electroweak symmetry breaking. In the remaining three cases, the pseudoscalar fields can obtain vacuum expectation values at different phases of the multi-step phase transition process, leading to spontaneous breaking of the CP symmetry. As the temperature decreases, the phase shifts to the vacuum observed today via first-order electroweak phase transition, at this point, the vacuum expectation value of the pseudoscalar field returns to zero, restoring the CP symmetry. Finally, we compare the transition strength and the stochastic gravitational wave background generated in the four situations along with the projected detection limits.

I. INTRODUCTION

In the intersecting of particle physics and cosmology, exploring a natural explanation for baryon asymmetry of the universe (BAU) [1] remains a challenging topic. Three Sakharov conditions must be satisfied for a dynamical generation of BAU: baryon number violation, C and CP violation, and departure from thermal equilibrium [2]. Among the mechanisms [3–8], the electroweak baryogenesis is an attractive mechanism for explaining the BAU due to its testability at the LHC and at the precision frontier by the electric dipole moment (EDM) experiments. The condition of departure from thermal equilibrium is met via a strong first-order electroweak phase transition (PT) [9, 10]. However, the electroweak PT in the SM is a crossover [11, 12], and the CP violation provided by the CKM matrix is too small to explain the observed BAU [13]. Therefore, the SM needs to be extended to provide large CP violation and a strong first-order electroweak PT, such as the singlet extension of SM (see e.g. [14–27]), the two-Higgs-doublet model (2HDM) and its extensions (see e.g. [28–43, 45, 46]). Adding explicit CP violation to these models can affect the EDM, which is constrained by negative results from electron EDM searches [47]. A finite temperature spontaneous CP violation mechanism can produce sufficient large CP violation while satisfying the EDM data naturally. Here, the CP symmetry is spontaneously broken at high temperature and restored in the current universe. The interesting mechanism has been implemented in the singlet scalar extension of the SM [23, 24], the singlet pseudoscalar extension of 2HDM (2HDM+***a***) [48, 49] and the complex singlet scalar extension of 2HDM [50, 51].

In the 2HDM+***a***, mixing between the singlet pseudoscalar and the Higgs doublet pseudoscalar occurs at zero temperature. At high temperature, these pseudoscalar fields acquire nonzero vacuum expectation value (VEV) leading to spontaneous CP symmetry breaking. This process can generate the observed BAU during a strong first-order electroweak PT. Ultimately, the observed vacuum state emerges, restoring CP symmetry at present temperatures. In Ref. [48, 49], the high-temperature approximation of the effective potential is taken to analyze the PT, which includes only the tree-level scalar potential and thermal masses of background fields.

In this work, we analyze the PTs in 2HDM+***a*** using the full one-loop finite-temperature effective potential which includes the tree-level potential, the Coleman-Weinberg term [52,

53] and the finite-temperature corrections [54]. We employ the $\overline{\text{MS}}$ scheme to handle the one-loop corrected tadpole conditions and Higgs masses, avoiding the infrared divergences associated with Goldstone boson loops that arise in the on-shell scheme. The model exhibits various PT patterns, including several multi-step PTs that deserve further detailed study. A first-order PT can generate detectable stochastic gravitational wave (GW) signals, which provide a new approach to search for new physics [55]. Compared to single-step PT, multi-step PTs can generate more diverse ranges of GW signals, with broader features in peak amplitude and frequency.

This paper is organized as follows: In Section II, we provide a review of the 2HDM+*a* and present the full one-loop finite-temperature effective potential. In Section III, we introduce theoretical and experimental constraints on the parameter space of the model. In Section IV, we discuss four different types of PTs and illustrate the evolution of the universe. In Section V, we numerically assess the potential of future GW detectors to probe the multi-step PTs identified in our work. Finally, we present our conclusion in Section VI.

II. 2HDM+*a* AND THE FINITE TEMPERATURE EFFECTIVE POTENTIAL

We extend the 2HDM by a pseudoscalar singlet field, whose tree-level potential is written as

$$\begin{aligned}
V_0(\Phi_1, \Phi_2, S) = & m_{11}^2 \left(\Phi_1^\dagger \Phi_1 \right) + m_{22}^2 \left(\Phi_2^\dagger \Phi_2 \right) - \left[m_{12}^2 \Phi_1^\dagger \Phi_2 + \text{h.c.} \right] \\
& + \frac{\lambda_1}{2} \left(\Phi_1^\dagger \Phi_1 \right)^2 + \frac{\lambda_2}{2} \left(\Phi_2^\dagger \Phi_2 \right)^2 + \lambda_3 \left(\Phi_1^\dagger \Phi_1 \right) \left(\Phi_2^\dagger \Phi_2 \right) \\
& + \lambda_4 \left(\Phi_1^\dagger \Phi_2 \right) \left(\Phi_2^\dagger \Phi_1 \right) + \left[\frac{\lambda_5}{2} \left(\Phi_1^\dagger \Phi_2 \right)^2 + \text{h.c.} \right] \\
& + \frac{1}{2} m_0^2 S^2 + \frac{\kappa_S}{24} S^4 + \left[i\mu S \Phi_2^\dagger \Phi_1 + \text{h.c.} \right] + \frac{\kappa_1}{2} S^2 \Phi_1^\dagger \Phi_1 + \frac{\kappa_2}{2} S^2 \Phi_2^\dagger \Phi_2.
\end{aligned} \tag{1}$$

To maintain the CP conservation, we assume all the mass and couplings parameters are real, and the singlet field S has no VEV at zero temperature. The Φ_1 and Φ_2 are the two Higgs-doublet fields,

$$\Phi_1 = \begin{pmatrix} \phi_1^+ \\ \frac{1}{\sqrt{2}} (v_1 + \phi_1 + i\eta_1) \end{pmatrix}, \quad \Phi_2 = \begin{pmatrix} \phi_2^+ \\ \frac{1}{\sqrt{2}} (v_2 + \phi_2 + i\eta_2) \end{pmatrix} \tag{2}$$

where v_1 and v_2 are VEVs with $v^2 = v_1^2 + v_2^2 = (246 \text{ GeV})^2$, and the ratio of the two VEVs is defined as

$$\tan \beta \equiv \frac{v_2}{v_1}. \quad (3)$$

The general Yukawa interactions at tree-level order are written as

$$\begin{aligned} -\mathcal{L} = & Y_{u1} \bar{Q}_L \tilde{\Phi}_1 u_R + Y_{u2} \bar{Q}_L \tilde{\Phi}_2 u_R \\ & + Y_{d1} \bar{Q}_L \Phi_1 d_R + Y_{d2} \bar{Q}_L \Phi_2 d_R \\ & + Y_{l1} \bar{L}_L \Phi_1 e_R + Y_{l2} \bar{L}_L \Phi_2 e_R + h.c., \end{aligned} \quad (4)$$

where $Q_L^T = (u_L, d_L)$, $L_L^T = (\nu_L, l_L)$, $\tilde{\Phi}_k = i\tau_2 \Phi_k^*$ with $k = 1, 2$. The elements of Y_{uk} , Y_{dk} and Y_{lk} determine the interactions between different scalar fields and fermions. We assume the Yukawa interactions to be aligned in order to prevent the tree-level flavour changing neutral current [56, 57],

$$\begin{aligned} (Y_{u1})_{ii} &= \frac{\sqrt{2}m_{ui}}{v} (c_\beta - s_\beta \kappa_u), \quad (Y_{u2})_{ii} = \frac{\sqrt{2}m_{ui}}{v} (s_\beta + c_\beta \kappa_u), \\ (Y_{l1})_{ii} &= \frac{\sqrt{2}m_{li}}{v} (c_\beta - s_\beta \kappa_l), \quad (Y_{l2})_{ii} = \frac{\sqrt{2}m_{li}}{v} (s_\beta + c_\beta \kappa_l), \\ (X_{d1})_{ii} &= \frac{\sqrt{2}m_{di}}{v} (c_\beta - s_\beta \kappa_d), \quad (X_{d2})_{ii} = \frac{\sqrt{2}m_{di}}{v} (s_\beta + c_\beta \kappa_d). \end{aligned} \quad (5)$$

$i = 1, 2, 3$ is the index of generation and $X_{d1,2} = V_{dL}^\dagger Y_{d1,2} V_{dR}$ with $V_{dL} \equiv V_{CKM}$. The unitary matrices $V_{dL,R}$ transform the original eigenstates to the mass eigenstates for the left-handed and right-handed down-type quark fields.

We analyze the phase histories of the model in the classical field space spanned by

$$\langle \Phi_1 \rangle = \begin{pmatrix} 0 \\ \frac{1}{\sqrt{2}} h_1 \end{pmatrix}, \quad \langle \Phi_2 \rangle = \begin{pmatrix} 0 \\ \frac{1}{\sqrt{2}} (h_2 + i h_3) \end{pmatrix}, \quad \langle S \rangle = h_4. \quad (6)$$

Here we take the imaginary part of the neutral elements of $\langle \Phi_1 \rangle$ to be zero. This choice is reasonable since the potential of Eq. (1) only depends on the relative phase of the neutral elements of $\langle \Phi_1 \rangle$ and $\langle \Phi_2 \rangle$.

The Higgs potential is modified from its tree-level form by the radiative corrections. At zero temperature, the effective potential at the one-loop level is written as,

$$V_{\text{eff}, T=0}(h_1, h_2, h_3, h_4) = V_0(h_1, h_2, h_3, h_4) + V_{\text{CW}}(h_1, h_2, h_3, h_4) \quad (7)$$

where V_0 is the tree-level potential, and V_{CW} is the Coleman-Weinberg (CW) potential. The V_0 is written as,

$$\begin{aligned} V_0(h_1, h_2, h_3, h_4) = & \frac{1}{2}m_{11}^2 h_1^2 + \frac{1}{2}m_{22}^2 h_2^2 + \frac{1}{2}m_{22}^2 h_3^2 - m_{12}^2 h_1 h_2 \\ & + \frac{1}{8}\lambda_1 h_1^4 + \frac{1}{8}\lambda_2 h_2^4 + \frac{1}{8}\lambda_2 h_3^4 + \frac{1}{4}h_2^2 h_3^2 \lambda_2 + \frac{1}{4}h_1^2 h_2^2 \lambda_{345} + \frac{1}{4}h_1^2 h_3^2 k_{345} \\ & + \mu h_1 h_3 h_4 + \frac{1}{2}m_0^2 h_4^2 + \frac{\kappa_S}{24}h_4^4 + \frac{\kappa_1}{4}h_4^2 h_1^2 + \frac{\kappa_2}{4}h_4^2 (h_2^2 + h_3^2), \end{aligned} \quad (8)$$

where $k_{345} = \lambda_3 + \lambda_4 - \lambda_5$ and $\lambda_{345} = \lambda_3 + \lambda_4 + \lambda_5$.

The V_{CW} in the $\overline{\text{MS}}$ renormalization scheme is given by [53]

$$V_{\text{CW}}(h_1, h_2, h_3, h_4) = \sum_i (-1)^{2s_i} n_i \frac{\hat{m}_i^4(h_1, h_2, h_3, h_4)}{64\pi^2} \left[\ln \frac{\hat{m}_i^2(h_1, h_2, h_3, h_4)}{Q^2} - C_i \right], \quad (9)$$

Q is a renormalization scale, and we take $Q^2 = v^2$. \hat{m}_i is the background-field-dependent mass of the neutral scalars (h, H, A, \mathbf{a}, G), the charged scalars (H^\pm, G^\pm), the heavy SM quark (t) and the gauge bosons (Z, W^\pm). The expression of \hat{m}_i can be found in the Appendix A. s_i is the spin of particle i , and the constant $C_i = \frac{3}{2}$ for scalars or fermions and $C_i = \frac{5}{6}$ for gauge bosons. n_i is the number of degree of freedom,

$$\begin{aligned} n_h &= n_H = n_A = n_{\mathbf{a}} = n_G = 1, \\ n_{H^\pm} &= n_{G^\pm} = 2, \\ n_{W^\pm} &= 6, \quad n_Z = 3, \\ n_t &= 12. \end{aligned} \quad (10)$$

We choose the $\overline{\text{MS}}$ renormalization scheme and the Landau gauge for the one-loop zero-temperature effective potential Eq. (7). The one-loop corrected tadpole conditions,

$$\begin{aligned} \left\langle \frac{\partial(V_0 + V_{\text{CW}})}{\partial h_1} \right\rangle &= 0, \\ \left\langle \frac{\partial(V_0 + V_{\text{CW}})}{\partial h_2} \right\rangle &= 0. \end{aligned} \quad (11)$$

The angle bracket $\langle \dots \rangle$ denotes the corresponding field-dependent values evaluated at the chosen true vacuum ($h_1 = v_1$, $h_2 = v_2$, $h_3 = 0$, and $h_4 = 0$) at zero temperature.

The one-loop improved mass squared matrices of the CP-even scalars, the charged scalars, and the CP-odd scalars are

$$\begin{pmatrix} \frac{\partial^2(V_0 + V_{\text{CW}})}{\partial h_1^2} & \frac{\partial^2(V_0 + V_{\text{CW}})}{\partial h_1 \partial h_2} \\ \frac{\partial^2(V_0 + V_{\text{CW}})}{\partial h_2 \partial h_1} & \frac{\partial^2(V_0 + V_{\text{CW}})}{\partial h_2^2} \end{pmatrix} = \begin{pmatrix} c_\alpha & -s_\alpha \\ s_\alpha & c_\alpha \end{pmatrix} \begin{pmatrix} m_H^2 & 0 \\ 0 & m_h^2 \end{pmatrix} \begin{pmatrix} c_\alpha & s_\alpha \\ -s_\alpha & c_\alpha \end{pmatrix}, \quad (12)$$

$$\begin{pmatrix} \frac{\partial^2(V_0+V_{\text{CW}})}{\partial G^+ \partial G^-} & \frac{\partial^2(V_0+V_{\text{CW}})}{\partial G^+ \partial H^-} \\ \frac{\partial^2(V_0+V_{\text{CW}})}{\partial H^+ \partial G^-} & \frac{\partial^2(V_0+V_{\text{CW}})}{\partial H^+ \partial H^-} \end{pmatrix} = \begin{pmatrix} c_\beta & s_\beta \\ -s_\beta & c_\beta \end{pmatrix} \begin{pmatrix} m_{G^\pm}^2 & 0 \\ 0 & m_{H^\pm}^2 \end{pmatrix} \begin{pmatrix} c_\beta & -s_\beta \\ s_\beta & c_\beta \end{pmatrix}, \quad (13)$$

$$\begin{pmatrix} \frac{\partial^2(V_0+V_{\text{CW}})}{\partial G^2} & \frac{\partial^2(V_0+V_{\text{CW}})}{\partial G \partial h_3} & \frac{\partial^2(V_0+V_{\text{CW}})}{\partial G \partial h_4} \\ \frac{\partial^2(V_0+V_{\text{CW}})}{\partial h_3 \partial G} & \frac{\partial^2(V_0+V_{\text{CW}})}{\partial h_3^2} & \frac{\partial^2(V_0+V_{\text{CW}})}{\partial h_3 \partial h_4} \\ \frac{\partial^2(V_0+V_{\text{CW}})}{\partial h_4 \partial G} & \frac{\partial^2(V_0+V_{\text{CW}})}{\partial h_4 \partial h_3} & \frac{\partial^2(V_0+V_{\text{CW}})}{\partial h_4^2} \end{pmatrix} = U \begin{pmatrix} m_G^2 & 0 & 0 \\ 0 & m_A^2 & 0 \\ 0 & 0 & m_a^2 \end{pmatrix} U^T, \quad (14)$$

with

$$U = \begin{pmatrix} c_\beta & s_\beta & 0 \\ -c_\theta s_\beta & c_\beta c_\theta & -s_\theta \\ -s_\beta s_\theta & c_\beta s_\theta & c_\theta \end{pmatrix}. \quad (15)$$

After solving the renormalization equations Eq. (11) to Eq. (14), the potential parameters in Eq. (1) are determined, and the background-field-dependent masses no longer satisfying tree-level relations, particularly $m_{G,G^\pm}^2 \neq 0$. Therefore, the second derivative of V_{CW} is free from infrared divergence [60, 61], avoiding the infrared divergences associated with Goldstone boson loops that arise in the on-shell scheme.

The physical scalar states are two neutral CP-even states h and H , two neutral pseudoscalars A and \mathbf{a} , and a pair of charged scalars H^\pm . Their Yukawa couplings are given by

$$\begin{aligned} -\mathcal{L}_Y = & \frac{m_f}{v} (\sin(\beta - \alpha) + \cos(\beta - \alpha) \kappa_f) h \bar{f} f \\ & + \frac{m_f}{v} (\cos(\beta - \alpha) - \sin(\beta - \alpha) \kappa_f) H \bar{f} f \\ & - i \frac{m_u}{v} \kappa_u c_\theta A \bar{u} \gamma_5 u + i \frac{m_d}{v} \kappa_d c_\theta A \bar{d} \gamma_5 d + i \frac{m_l}{v} \kappa_l c_\theta A \bar{l} \gamma_5 l \\ & - i \frac{m_u}{v} \kappa_u s_\theta \mathbf{a} \bar{u} \gamma_5 u + i \frac{m_d}{v} \kappa_d s_\theta \mathbf{a} \bar{d} \gamma_5 d + i \frac{m_l}{v} \kappa_l s_\theta \mathbf{a} \bar{l} \gamma_5 l \\ & + H^+ \bar{u} V_{CKM} \left(\frac{\sqrt{2} m_d}{v} \kappa_d P_R - \frac{\sqrt{2} m_u}{v} \kappa_u P_L \right) d + \text{h.c.} \\ & + \frac{\sqrt{2} m_l}{v} \kappa_l H^+ \bar{v} P_R e + \text{h.c..} \end{aligned} \quad (16)$$

At finite temperatures, the thermal corrections to the potential become important. Here we use the one-loop correction [54],

$$\begin{aligned} V_{\text{th}}(h_1, h_2, h_3, h_4, T) &= \frac{T^4}{2\pi^2} \sum_i n_i J_{B,F} \left(\frac{\hat{m}_i^2(h_1, h_2, h_3, h_4)}{T^2} \right), \\ J_{B,F}(y) &= \pm \int_0^\infty dx x^2 \ln \left[1 \mp \exp \left(-\sqrt{x^2 + y} \right) \right]. \end{aligned} \quad (17)$$

In this work we employ the Parwani method [62] to handle the daisy diagrams [63]. This involves replacing the mass $\hat{m}_i^2(h_1, h_2, h_3, h_4)$ with the thermal Debye mass $\bar{M}_i^2(h_1, h_2, h_3, h_4, T)$. The thermal Debye masses for $h, H, A, \mathbf{a}, G, H^\pm, G^\pm, W_L^\pm, Z_L, \gamma_L$ can be found in Appendix A, where W_L^\pm , Z_L , and γ_L are the longitudinal gauge bosons with $n_{W_L^\pm} = 2$, $n_{Z_L} = n_{\gamma_L} = 1$.

III. THEORETICAL AND EXPERIMENTAL CONSTRAINTS

(1) Theoretical constraints. The requirement of vacuum stability ensures that the potential is bounded from below and that the electroweak vacuum is the global minimum of the full scalar potential. The unitarity constraint is applied to prevent theoretical $2 \rightarrow 2$ particle scattering processes from producing unphysical results. Detailed discussions on the vacuum stability and unitarity can be found in Ref. [64, 65], we employ the formulas in [64, 65] to implement the relevant theoretical constraints.

(2) The signal data of the 125 GeV Higgs. We take the light CP-even h as the observed 125 GeV Higgs, and $\sin(\beta - \alpha) \approx 1$ to be aligned to the SM Higgs coupling. This choice can avoid the constraints from the signal data of the 125 GeV Higgs.

(3) Searches for extra Higgses at the LHC and flavour physics constraints. The Yukawa couplings of the other Higgses (H, H^\pm, A, \mathbf{a}) are proportional to κ_u , κ_d and κ_ℓ when $\sin(\beta - \alpha) \approx 1$. Therefore, we assume κ_u , κ_d and κ_ℓ to be small enough to suppress the production cross sections of these Higgses at the LHC, and consistent with the exclusion limits of searches for additional Higgs bosons. Additionally, very small values of κ_u , κ_d and κ_ℓ satisfy the bounds from flavour physics observables.

(4) The oblique electroweak parameters. The oblique parameters (S, T, U) quantify the effects of electroweak symmetry breaking. Additional Higgs particles introduce new Feynman diagrams through interactions with W and Z bosons, impacting the S , T and U

parameters. The expressions for S , T and U in this model are [66, 67]

$$\begin{aligned}
S &= \frac{1}{\pi m_Z^2} [c_\theta^2 F_S(m_Z^2, m_H^2, m_A^2) + s_\theta^2 F_S(m_Z^2, m_H^2, m_a^2) - F_S(m_Z^2, m_{H^\pm}^2, m_{H^\pm}^2)], \\
T &= \frac{1}{16\pi m_W^2 s_W^2} [-c_\theta^2 F_T(m_H^2, m_A^2) - s_\theta^2 F_T(m_H^2, m_a^2) + F_T(m_{H^\pm}^2, m_H^2) \\
&\quad + c_\theta^2 F_T(m_{H^\pm}^2, m_A^2) + s_\theta^2 F_T(m_{H^\pm}^2, m_a^2)], \\
U &= \frac{1}{\pi m_W^2} [F_S(m_W^2, m_{H^\pm}^2, m_H^2) - 2F_S(m_W^2, m_{H^\pm}^2, m_{H^\pm}^2) \\
&\quad + c_\theta^2 F_S(m_W^2, m_{H^\pm}^2, m_A^2) + s_\theta^2 F_S(m_W^2, m_{H^\pm}^2, m_a^2) \\
&\quad - \frac{1}{\pi m_Z^2} [c_\theta^2 F_S(m_Z^2, m_H^2, m_A^2) + s_\theta^2 F_S(m_Z^2, m_H^2, m_a^2) - F_S(m_Z^2, m_{H^\pm}^2, m_{H^\pm}^2)]],
\end{aligned} \tag{18}$$

where

$$\begin{aligned}
F_T(a, b) &= \frac{1}{2}(a + b) - \frac{ab}{a - b} \log\left(\frac{a}{b}\right), \\
F_S(a, b, c) &= B_{22}(a, b, c) - B_{22}(0, b, c), \\
B_{22}(a, b, c) &= \frac{1}{4} \left[b + c - \frac{1}{3}a \right] - \frac{1}{2} \int_0^1 dx X \log(X - i), \\
X &= bx + c(1 - x) - ax(1 - x).
\end{aligned} \tag{19}$$

Based on the recent fitting results of Ref.[68], we use the following values of S , T and U

$$S = -0.01 \pm 0.10, \quad T = -0.03 \pm 0.12, \quad U = 0.02 \pm 0.11. \tag{20}$$

correction factor

$$\rho_{ST} = -0.92, \quad \rho_{SU} = -0.80, \quad \rho_{TU} = -0.93. \tag{21}$$

IV. ELECTROWEAK PHASE TRANSITION

We utilized the publicly available code **PhaseTracer** [69] for numerical analyses of PTs. This code traces the minima of the effective potential as temperature varies and calculates the critical temperatures T_c where these minima become degenerate. This approach helps us investigate the complex dynamics of PTs involving multiple scalar fields. We use γ as a metric to quantify the strength of a PT [70, 71], defined as:

$$\gamma \equiv \frac{v(T_c)}{T_c}, \tag{22}$$

where $v = \sqrt{h_1^2 + h_2^2 + h_3^2 + h_4^2}$ represents the VEV at true vacuum. To ensure that the current universe is in the observed electroweak symmetry breaking vacuum, we necessitate

	m_H (GeV)	m_A (GeV)	m_a (GeV)	m_0^2 (GeV) ²	κ_1	κ_2	κ_S	μ	$\tan \beta$
BP1	288.69	158.63	403.74	-129.95	5.13	5.28	6.35	-137.93	0.63
BP2	310.57	157.42	430.75	-136.72	5.95	5.05	6.62	180.23	0.60
BP3	330.75	150.69	478.25	-2978.50	3.22	8.49	8.73	-364.11	0.85
BP4	313.61	143.30	509.19	-4256.47	2.69	9.08	7.42	-448.85	0.87
BP5	350.60	153.47	475.76	-16812.75	3.18	8.76	7.65	-357.66	0.94
BP6	346.47	150.51	440.59	-19431.57	2.73	8.77	8.81	-320.14	0.81

TABLE I: The input parameters for the BPs. $m_H = m_{H^\pm}$ are chosen to satisfy the constraints from the oblique parameters.

that the vacuum characterized by $v = \sqrt{h_1^2 + h_2^2} = 246$ GeV and $h_3 = h_4 = 0$ is the deepest vacuum at zero temperature. The metastable electroweak symmetry breaking vacuum with a lifetime exceeding the age of the universe is not within the scope of this discussion.

We select six benchmark points (BPs) in the surviving parameter space to detail the physical processes associated with the PTs. The PT histories are illustrated in FIG. 1 to FIG. 6, which show the VEVs of the scalar fields as functions of temperature. Arrows in the figures indicate that at the critical temperatures, the two phases connected by the arrows are degenerate, implying the possibility of a first-order PT occurring along the direction of the arrow. Dots represent the vacuum fields that remain unchanged during the transition. The parameters for these BPs are provided in TABLE I, and T_c and PT strengths at each step are shown in TABLE II.

The PT types mentioned in Ref. [49], using high temperature approximation where CP symmetry is broken at high temperatures and restored at low temperatures, align with PB4 and BP5 found in our work. Additionally, we have identified two unique PT types, as specifically illustrated in FIG. 3 and FIG. 6. In the subsequent discussion, we categorize these PT processes into two distinct classes, based on whether the CP-symmetry is broken at a finite temperature.

A. CP symmetry conserved at all temperatures.

For the scenarios described by the BP1 and BP2, only the field configurations h_1 and h_2 acquire non-zero VEVs and break the electroweak symmetry, while the VEVs of other fields

	T_{c1}	γ_1	T_{c2}	γ_2	T_{c3}	γ_3
BP1	115.75	1.23	-	-	-	-
BP2	110.89	1.44	-	-	-	-
BP3	165.64	0.39	96.01	2.18	-	-
BP4	181.86	0.45	89.15	2.54	-	-
BP5	99.35	2.08	94.45	2.26	-	-
BP6	116.37	1.24	96.56	2.29	92.04	2.44

TABLE II: Critical temperatures and strengths of the PTs for BPs.

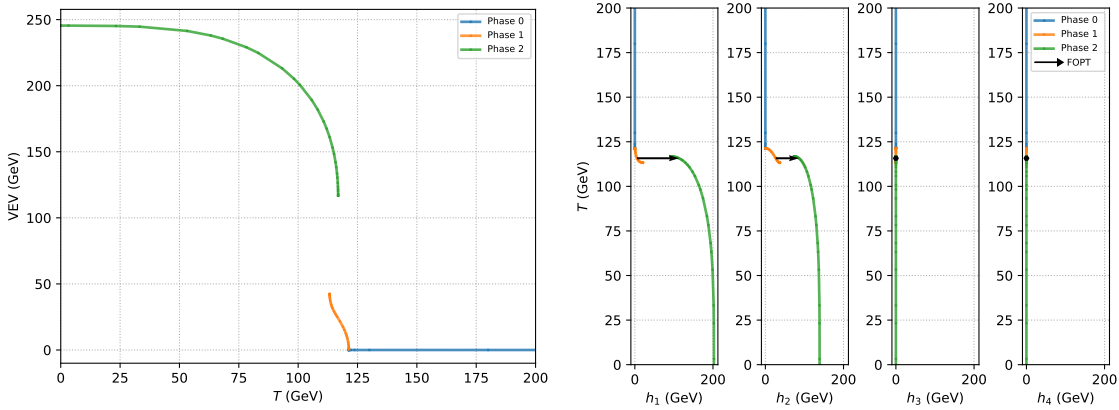


FIG. 1: Phase histories for BP1. The black arrows depict the critical temperatures, hinting at the possibility of a FOPT occurring in the direction of the arrows. The dots, on the other hand, signify that the corresponding vacuum field remains unchanged during the transition.

keep zero. So under these scenarios the CP symmetry is conservation in the whole thermal history. In the BP1 scenario, electroweak symmetry is firstly broken through a cross-over transition, which is characterized by the continuous evolution of the effective potential's minima, as shown in FIG. 1, illustrating the shift from Phase 0 to Phase 1. The system evolves in Phase 1 until the temperature drops to 115.75 GeV, and then the minima of the effective potential has two different values in Phase 1 and Phase 2 respectively. A strong first-order electroweak PT takes place and the PT strength is greater than one. In the BP2 scenario, the Universe undergoes a single-step process, which is a strong first-order electroweak PT with critical temperature $T_{c1} = 110.89$ GeV and PT strength $\gamma_1 = 1.44$.

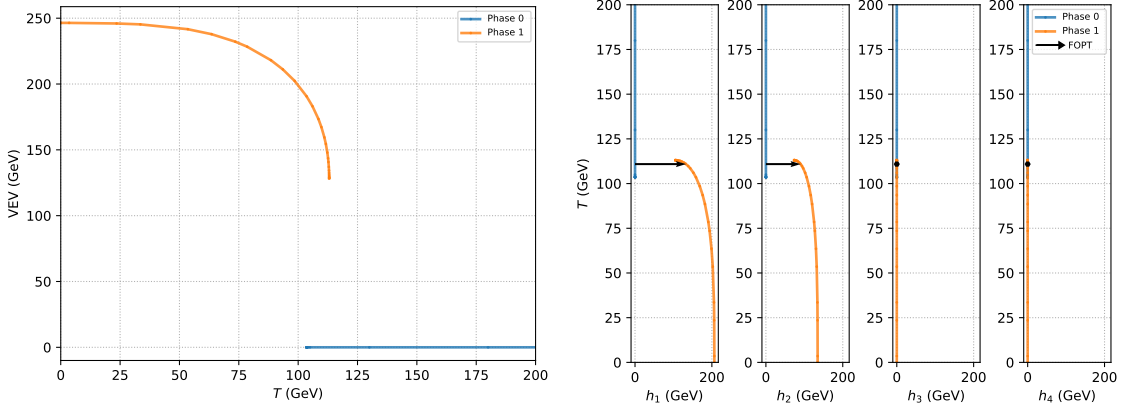


FIG. 2: Same as Fig. 1, but for BP2.

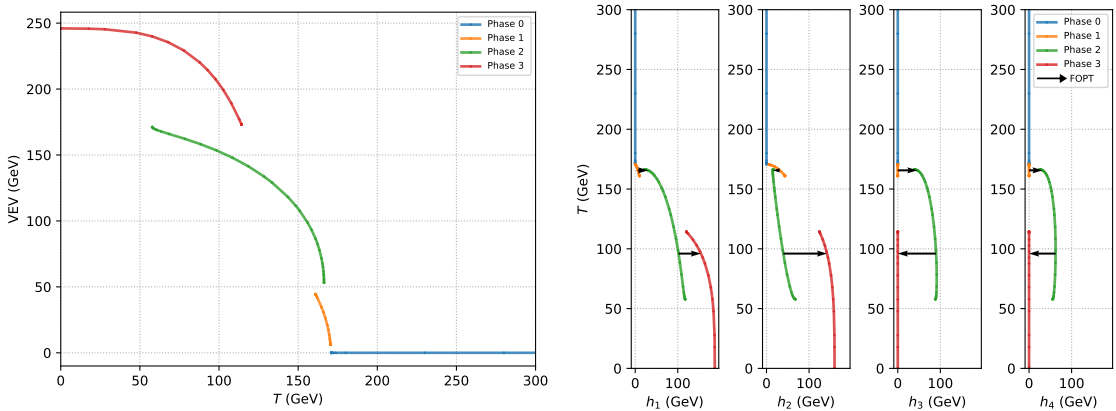


FIG. 3: Same as Fig. 1, but for BP3.

B. CP symmetry broken at high temperatures and recovered at the present temperatures.

Unlike the scenario discussed above, we now turn to the special cases described by BP3 to BP6. In these cases, the CP-odd Higgs fields h_3 and h_4 acquire nonzero VEVs at high temperatures but return to zero as the temperature decreases. Thus, the CP symmetry is spontaneously broken at high temperature and then restored at the present temperatures.

- Electroweak and CP symmetries broken in sequence.

Now we will describe the process of BP3 in detail. As shown in the right panel of FIG. 3, in Phase 1 h_1 and h_2 acquire non-zero VEVs through a cross-over PT and break the electroweak symmetry spontaneously, while the CP symmetry remains conserved since the configurations of CP-odd Higgs fields do not acquire non-zero VEVs. However, when the

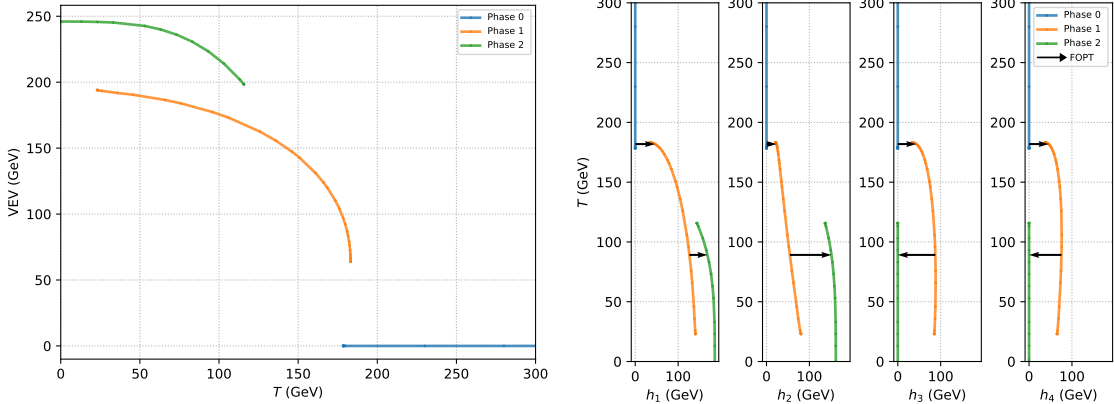


FIG. 4: Same as Fig. 1, but for BP4.

temperature decreases to 165.64 GeV, the CP symmetry is broken as h_3 and h_4 acquire non-zero VEVs. This marks a first-order electroweak PT from Phase 1 to Phase 2. Subsequently, as the temperature drop further to 96.01 GeV, the system tunnels from Phase 2 to Phase 3 via a strong first-order electroweak PT. The VEVs of the four fields ($\langle h_1 \rangle, \langle h_2 \rangle, \langle h_3 \rangle, \langle h_4 \rangle$) shift from (101.80, 39.44, 90.05, 62.38) GeV to (154.51, 142.32, 0.0, 0.0) GeV. In this final phase, the CP symmetry is recovered. The system continues to evolve along the last phase, eventually settling into the observed vacuum state.

- Electroweak and CP symmetry broken Together

The PT process of BP4 is similar to the second and third steps of BP3 scenario. A degenerate state appears between Phase 0 and Phase 1 at the critical temperature T_{c1} . After this, h_1 , h_2 , h_3 and h_4 acquire non-zero VEVs, indicating a new phase where both electroweak and CP symmetries are broken. In Phase 1, the VEVs of the four fields gradually increase as the temperature decreases. The second PT occurs at $T_{c2} = 89.15$ GeV, at which the system undergoes a strong first-order electroweak PT, tunneling into the final phase and restoring the CP symmetry.

- CP symmetry broken before electroweak symmetry.

For the BP5 the Universe undergoes five different phases, and two cross-over PTs takes place from Phase 0 to Phase 2. In Phase 1, the CP symmetry is broken spontaneously when the h_4 field acquires a non-zero VEV while the VEVs of h_1 and h_2 remain zero, respecting electroweak symmetry. In Phase 2, the remaining fields, especially h_1 and h_2 , acquire non-zero VEVs and break the electroweak symmetry spontaneously. Both Phase 2 and Phase

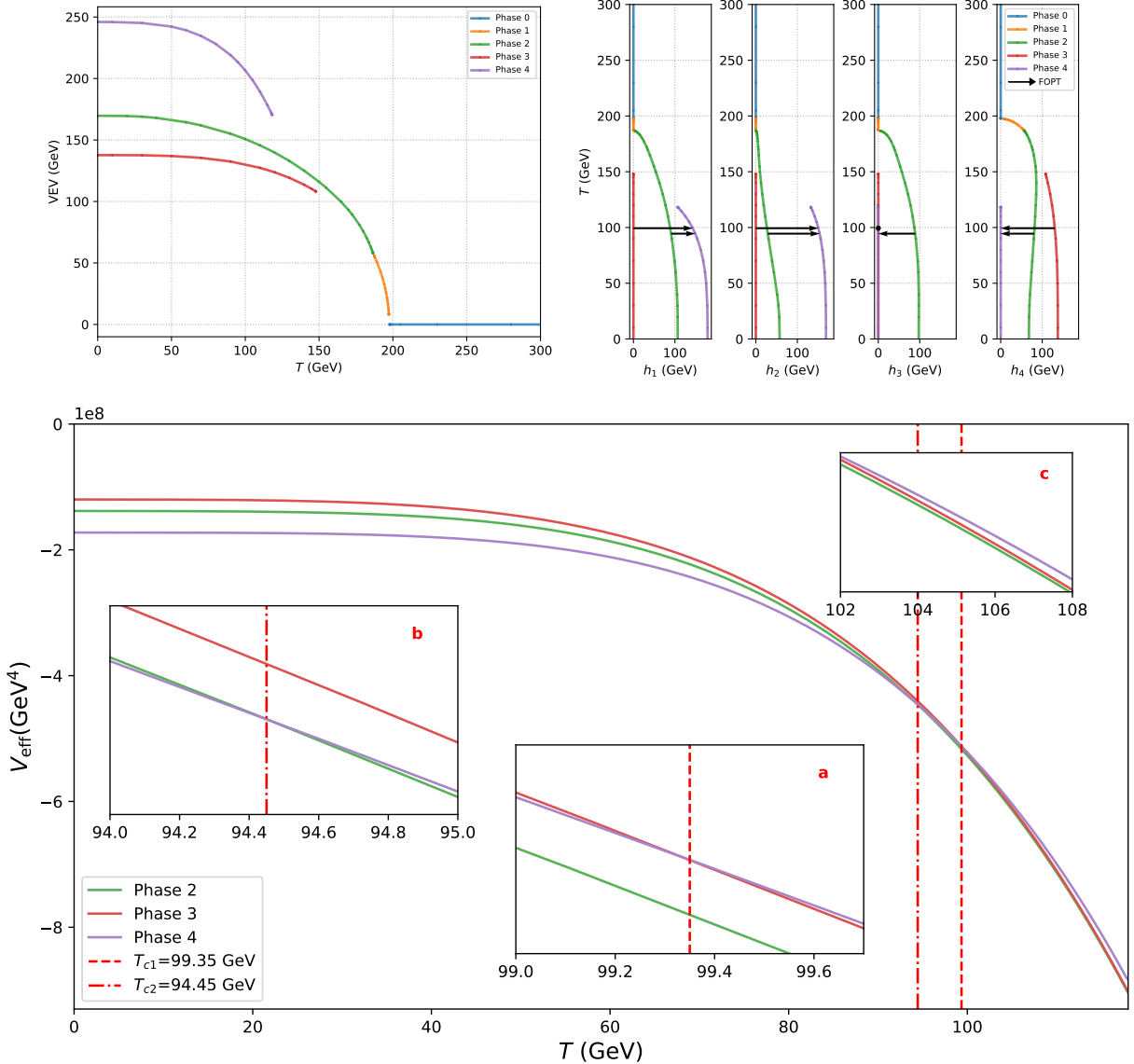


FIG. 5: **Top:** Same as Fig. 1, but for BP5. **Bottom:** The variation of the effective potential as function of temperature across different phases.

3 represent unstable false vacuum and the system will tunnel into the final phase by two strong first-order electroweak PTs. Phase 4 is the final phase, where the VEVs of h_3 and h_4 return to zero, restoring the CP symmetry. Ultimately, the observed vacuum is obtained as the temperature approaches zero.

In the bottom panel of FIG. 5, the effective potential variations across Phases 2, 3 and 4 are represented by the green, red, and purple lines, respectively. The curves of Phase 3 (Phase 2) intersect with Phase 4 at $T = 99.35$ GeV ($T = 94.45$ GeV), as shown in subplot

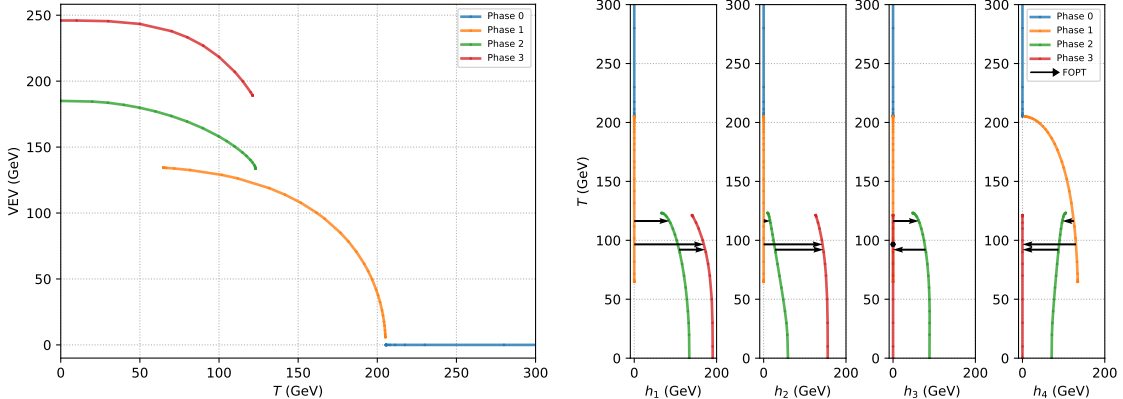


FIG. 6: Same as Fig. 1, but for BP6

(a) (subplot (b)). These intersection points highlight the presence of critical temperatures. In subplot (c), the effective potential of Phase 2 is lower than that of Phase 3, and this characteristic persists as the temperature decreases to zero, so no PT occurs between these two phases.

BP6 exhibits two potential transition pathways: (i) sequential transitions, proceeding first from Phase 1 to Phase 2, and subsequently from Phase 2 to Phase 3, and (ii) direct transitions from Phase 1 to Phase 3, bypassing Phase 2. This is quite distinct from previous benchmark points and may yield a rich phenomenology. The calculation of their transition probabilities requires special consideration and is left for future research.

V. GRAVITATIONAL WAVE

During the first-order PT, the GW can be generated, which has three primary sources: bubble collisions, plasma sound waves and magnetohydrodynamic turbulence. Bubble collisions becomes significant when the bubble wall velocity \tilde{v}_W approaches the speed of light. Here we focus on plasma sound waves and magnetohydrodynamic turbulence as the dominant contributors to GW production in our subsequent calculations.

The contribution originating from the sound waves can be expressed by [72]

$$\begin{aligned} \Omega_{\text{sw}} h^2 &= 2.65 \times 10^{-6} \left(\frac{H(T_*)}{\beta} \right) \left(\frac{\kappa_{\text{sw}} \alpha}{1 + \alpha} \right)^2 \left(\frac{100}{g_*(T_*)} \right)^{1/3} \tilde{v}_W \\ &\times \left(\frac{f}{f_{\text{sw}}} \right)^3 \left(\frac{7}{4 + 3(f/f_{\text{sw}})^2} \right)^{7/2} \Upsilon(\tau_{\text{sw}}), \end{aligned} \quad (23)$$

we take $\tilde{v}_W = 0.6$ in our calculation [73]. $H(T_*)$ is the Hubble parameter at reference

temperature T_* . $g_*(T_*)$ is the effective number of relativistic degrees of freedom at T_* . The κ_{sw} is the fraction of latent heat transformed into the kinetic energy of the fluid [74]. The suppression factor $\Upsilon(\tau_{\text{sw}})$ is a function of the lifetime of the source [75].

$$\Upsilon(\tau_{\text{sw}}) = 1 - \frac{1}{\sqrt{1 + 2\tau_{\text{sw}}H_n}} , \quad (24)$$

arises due to the finite lifetime τ_{sw} of the sound waves [76, 77],

$$\tau_{\text{sw}} = \frac{\tilde{v}_W(8\pi)^{1/3}}{\beta\bar{U}_f}, \quad \bar{U}_f^2 = \frac{3}{4} \frac{\kappa_{\text{sw}}\alpha}{1 + \alpha} . \quad (25)$$

α is the transition strength parameter, define as the ratio of the vacuum energy density released during the PT to the total radiation energy density at the reference temperature.

$$\alpha = \frac{1}{\pi^2 g_*(T) T^4 / 30} \left(\Delta V_{\text{eff}} - \frac{T}{4} \frac{d\Delta V_{\text{eff}}}{dT} \right) |_{T=T_*} , \quad (26)$$

β represents the inverse of the time duration of the PT,

$$\beta = TH(T) \frac{d(S_3/T)}{dT} |_{T=T_*} . \quad (27)$$

S_3 is the three-dimensional Euclidean action. f_{sw} is the present peak frequency of the spectrum,

$$f_{\text{sw}} = 1.9 \times 10^{-5} \frac{1}{\tilde{v}_W} \left(\frac{\beta}{H(T_*)} \right) \left(\frac{T_*}{100\text{GeV}} \right) \left(\frac{g_*(T_*)}{100} \right)^{1/6} \text{Hz} . \quad (28)$$

The contribution from the turbulence can be expressed by [78, 79]

$$\begin{aligned} \Omega_{\text{turb}} h^2 &= 3.35 \times 10^{-4} \left(\frac{H(T_*)}{\beta} \right) \left(\frac{\kappa_{\text{turb}}\alpha}{1 + \alpha} \right)^2 \left(\frac{100}{g_*(T_*)} \right)^{1/3} \tilde{v}_W \\ &\times \frac{(f/f_{\text{turb}})^3}{(1 + f/f_{\text{turb}})^{11/3} (1 + 8\pi f/H_0)} , \end{aligned} \quad (29)$$

we take $\kappa_{\text{turb}} \approx 0.1 \kappa_{\text{sw}}$ and the H_0 is

$$H_0 = 1.65 \times 10^{-5} \left(\frac{T_*}{100\text{GeV}} \right) \left(\frac{g_*(T_*)}{100} \right)^{1/6} . \quad (30)$$

The present peak frequency

$$f_{\text{turb}} = 2.7 \times 10^{-5} \frac{1}{\tilde{v}_W} \left(\frac{\beta}{H(T_*)} \right) \left(\frac{T_*}{100\text{GeV}} \right) \left(\frac{g_*(T_*)}{100} \right)^{1/6} \text{Hz} . \quad (31)$$

In Section IV we set the reference temperature to the critical temperature T_c to analyze multi-step PTs. When the the universe's temperature drops below T_c , bubbles form in the

	T_{n1}	T_{n2}	T_{n3}
BP1	114.92	-	-
BP2	108.52	-	-
BP3	161.01	84.36	-
BP4	178.40	73.41	-
BP5	-	73.08	-
BP6	103.95	-	72.45

TABLE III: Nucleation temperatures of BP1 to BP6.

unstable false vacuum. The nucleation temperature T_n is commonly regarded as the starting point of the PT. We use T_n as the reference temperature T_* to examine the production of the stochastic GW background. Bubble nucleation is a stochastic process, and the nucleation rate per unit volume and time is given by $\Gamma = A e^{-S_3/T}$, where A is typically approximated as the fourth power of the temperature at high temperatures.

The total number of bubbles within a Hubble volume, from the critical moment T_c to T_n , is of the order of $\mathcal{O}(1)$ [80],

$$\int_{T_c}^{T_n} \frac{dT}{T} \left(\frac{90}{\pi^2 g_*(T)} \right)^2 \left(\frac{m_{\text{pl}}}{T} \right)^4 e^{-S_3(T)/T} = \mathcal{O}(1). \quad (32)$$

In our discussion of first-order fast PT at the electroweak scale, the integrals can be roughly approximated as being dominated by their value at T_n . $g_*(T_n) \approx 106.75$ and m_{pl} is the approximate Planck mass in the natural system of units, i.e. $m_{\text{pl}} = 2.4 \times 10^{18}$ GeV. Thus, Eq. (32) is approximately satisfied for $S_3(T_n)/T_n \approx 140$. In spherical coordinates, S_3 is given by [81],

$$S_3 = 4\pi \int_o^{\infty} dr r^2 \left[\sum_{i=1}^4 \frac{1}{2} \left(\frac{dh_i}{dr} \right)^2 + V_{\text{eff}} \right]. \quad (33)$$

The field configurations can be solved via the bounce equations,

$$\frac{d^2 h_i}{dr^2} + \frac{2}{r} \frac{dh_i}{dr} = \frac{\partial V_{\text{eff}}}{\partial h_i}, \quad (i = 1, 2, 3, 4). \quad (34)$$

We use the publicly code **CosmoTransition** [82] to compute S_3 . TABLE III shows the T_n calculated by **CosmoTransition** for various BP scenarios.

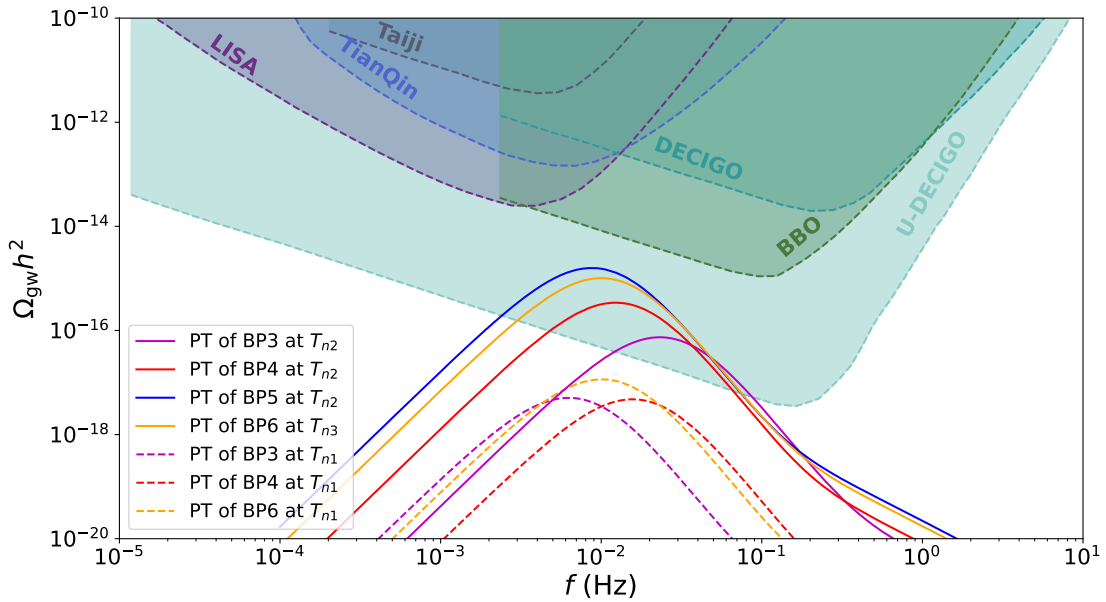


FIG. 7: The gravitational wave spectra for the BP3, BP4, BP5 and BP6 compared with the expected sensitivities of Taiji, BBO, DECIGO, LISA, U-DECIGO and TianQin experiments, respectively.

In FIG. 7, we show the GW spectra for the benchmark points along with the sensitivity curves of LISA [83], Taiji [84], TianQin [85], Big Bang Observer (BBO) [86], DECi-hertz Interferometer GW Observatory (DECIGO) [86] and Ultimate-DECIGO (U-DECIGO) [87]. For BP1 and BP2, the peak spectrum values are below 10^{-20} , and consequently, they are not displayed in FIG. 7. The peak spectrum values for BP3, BP4 and BP5 at T_{n2} as well as for BP6 at T_{n3} , fall within the sensitivity range of U-DECIGO detectors, which have peak frequencies around 0.01 Hz. In contrast, the peak spectrum values for BP3, BP4, BP5 and BP6 at T_{n1} are relatively weak, with values of $\mathcal{O}(-17)$.

VI. CONCLUSION

We examined the multi-step PTs in the 2HDM+ α considering the $\overline{\text{MS}}$ scheme to renormalize the one-loop effective potential which effectively avoids the IR divergence associated with Goldstone boson loop. After considering both theoretical and experimental constraints on this model, we identify four classes of evolution processes with multi-step PTs. In the

first case, only the CP-even Higgs acquires a non-zero VEV via a first-order or cross-over PT, and breaks electroweak symmetry while the CP symmetry is always conserved. In the remaining three cases, the pseudoscalar fields can obtain VEVs at different phases of the multi-step PTs, leading to spontaneous breaking of the CP symmetry. As the temperature decreases, the observed vacuum at the present temperature is obtained via strong first-order electroweak PT and the CP symmetry is recovered. Finally, we compared the GW spectrum generated in the four scenarios with the projected detection limits. We found that the GW spectrum from the different step of the PT in BP3, BP4, BP5 and BP6 can be expected to reach the detection sensitivity of U-DECIGO.

Acknowledgments

We thank Yang Xiao for helpful discussions. This work was supported by the National Natural Science Foundation of China under grants, 11975013, 12105248, 12335005, the Natural Science Foundation of Shandong province ZR2023MA038, and Henan Postdoctoral Science Foundation HN2024003.

Appendix A: The background-field-dependent masses and the thermal Debye masses

We obtain the field-dependent masses of the scalars $h, H, A, \mathbf{a}, H^\pm$ and the Goldstone bosons G^\pm, G by

$$\begin{aligned}\hat{m}_{h,H,A,\mathbf{a},G}^2 &= \text{eigenvalues} \left(\hat{\mathcal{M}}_N^2 \right), \\ \hat{m}_{G^\pm,H^\pm}^2 &= \text{eigenvalues} \left(\hat{\mathcal{M}}_C^2 \right).\end{aligned}\tag{A1}$$

The $\hat{\mathcal{M}}_N^2$ denotes the mass matrix of the neutral Higgs,

$$\begin{aligned}\hat{\mathcal{M}}_{N11}^2 &= \frac{3\lambda_1}{2}h_1^2 + \frac{\lambda_{345}}{2}h_2^2 + \frac{k_{345}}{2}h_3^2 + m_{11}^2 + \frac{\kappa_1}{2}h_4^2, \\ \hat{\mathcal{M}}_{N22}^2 &= \frac{3\lambda_2}{2}h_2^2 + \frac{\lambda_2}{2}h_3^2 + \frac{\lambda_{345}}{2}h_1^2 + m_{22}^2 + \frac{\kappa_2}{2}h_4^2, \\ \hat{\mathcal{M}}_{N33}^2 &= \frac{\lambda_2}{2}h_2^2 + \frac{3\lambda_2}{2}h_3^2 + m_{22}^2 + \frac{k_{345}}{2}h_1^2 + \frac{\kappa_2}{2}h_4^2, \\ \hat{\mathcal{M}}_{N44}^2 &= m_0^2 + \frac{\kappa_1}{2}h_1^2 + \frac{\kappa_2}{2}h_2^2 + \frac{\kappa_2}{2}h_3^2 + \frac{\kappa_S}{2}h_4^2, \\ \hat{\mathcal{M}}_{N55}^2 &= \frac{\lambda_1}{2}h_1^2 + m_{11}^2 + \frac{k_{345}}{2}h_2^2 + \frac{\lambda_{345}}{2}h_3^2 + \frac{\kappa_1}{2}h_4^2, \\ \hat{\mathcal{M}}_{N12}^2 &= \hat{\mathcal{M}}_{N21}^2 = \lambda_{345}h_1h_2 - m_{12}^2, \\ \hat{\mathcal{M}}_{N13}^2 &= \hat{\mathcal{M}}_{N31}^2 = k_{345}h_1h_3 + h_4\mu, \\ \hat{\mathcal{M}}_{N14}^2 &= \hat{\mathcal{M}}_{N41}^2 = \kappa_1h_1h_4 + h_3\mu, \\ \hat{\mathcal{M}}_{N15}^2 &= \hat{\mathcal{M}}_{N51}^2 = h_2h_3\lambda_5, \\ \hat{\mathcal{M}}_{N23}^2 &= \hat{\mathcal{M}}_{N32}^2 = h_2h_3\lambda_2, \\ \hat{\mathcal{M}}_{N24}^2 &= \hat{\mathcal{M}}_{N42}^2 = \kappa_2h_2h_4, \\ \hat{\mathcal{M}}_{N25}^2 &= \hat{\mathcal{M}}_{N52}^2 = h_1h_3\lambda_5 - h_4\mu, \\ \hat{\mathcal{M}}_{N34}^2 &= \hat{\mathcal{M}}_{N43}^2 = \kappa_2h_3h_4 + h_1\mu, \\ \hat{\mathcal{M}}_{N35}^2 &= \hat{\mathcal{M}}_{N53}^2 = \lambda_5h_1h_2 - m_{12}^2, \\ \hat{\mathcal{M}}_{N45}^2 &= \hat{\mathcal{M}}_{N54}^2 = -h_2\mu.\end{aligned}\tag{A2}$$

At zero temperature, due to $\langle h_3 \rangle = 0$ and $\langle h_4 \rangle = 0$, the 5×5 matrix $\hat{\mathcal{M}}_N^2$ is reduced to one 2×2 matrix $\hat{\mathcal{M}}_P^2$ and one 3×3 matrix $\hat{\mathcal{M}}_O^2$, with the former denoting the mass matrix of the CP-even scalar and the latter denoting the mass matrix of the CP-odd scalar, respectively. When solving Eqs. (11) to (14), the background field also includes ϕ_1^\pm, ϕ_2^\pm and η_1 . The $\hat{\mathcal{M}}_C^2$

denotes the mass matrix of the charged Higgs,

$$\begin{aligned}\hat{\mathcal{M}}_{C11}^2 &= \frac{\lambda_1}{2}h_1^2 + m_{11}^2 + \frac{\lambda_3}{2}h_2^2 + \frac{\lambda_3}{2}h_3^2 + \frac{\kappa_1}{2}h_4^2, \\ \hat{\mathcal{M}}_{C22}^2 &= \frac{\lambda_2}{2}h_2^2 + \frac{\lambda_2}{2}h_3^2 + m_{22}^2 + \frac{\lambda_3}{2}h_1^2 + \frac{\kappa_2}{2}h_4^2, \\ \hat{\mathcal{M}}_{C12}^2 &= \left(\hat{\mathcal{M}}_{C21}^2\right)^\dagger = \frac{(\lambda_4 + \lambda_5)}{2}h_1h_2 - m_{12}^2 + ih_4\mu + i\frac{(\lambda_4 - \lambda_5)}{2}h_1h_3.\end{aligned}\tag{A3}$$

The field-dependent masses of the gauge bosons W^\pm, Z, γ are

$$\begin{aligned}\hat{m}_{W^\pm}^2 &= \frac{1}{4}g^2(h_1^2 + h_2^2 + h_3^2), \\ \hat{m}_Z^2 &= \frac{1}{4}(g^2 + g'^2)(h_1^2 + h_2^2 + h_3^2), \\ \hat{m}_\gamma^2 &= 0.\end{aligned}\tag{A4}$$

Neglecting the contribution of lighter fermions, we focus on the field-dependent masses of the top quark,

$$\hat{m}_t^2 = \frac{1}{2}y_t^2 \left[(h_1c_\beta + h_2s_\beta)^2 + h_3^2s_\beta^2\right],\tag{A5}$$

where $y_t = \sqrt{2}m_t/v$.

The thermal Debye masses $\bar{M}_i^2(h_1, h_2, h_3, h_4, T)$, where $i = h, H, A, \mathbf{a}, G, H^\pm, G^\pm$, are the eigenvalues of the full mass matrix,

$$\begin{aligned}\bar{M}_i^2(h_1, h_2, h_3, h_4, T) &= \text{eigenvalues} \left[\widehat{\mathcal{M}_X^2}(h_1, h_2, h_3, h_4) + \Pi_X(T) \right], \\ \Pi_{P11} &= \left[\frac{9g^2}{2} + \frac{3g'^2}{2} + 6y_t^2c_\beta^2 + 6\lambda_1 + 4\lambda_3 + 2\lambda_4 + \kappa_1 \right] \frac{T^2}{24}, \\ \Pi_{P22} &= \left[\frac{9g^2}{2} + \frac{3g'^2}{2} + 6y_t^2s_\beta^2 + 6\lambda_2 + 4\lambda_3 + 2\lambda_4 + \kappa_2 \right] \frac{T^2}{24}, \\ \Pi_{P33} &= \Pi_{P22}, \\ \Pi_{P44} &= [4\kappa_1 + 4\kappa_2 + \kappa_S] \frac{T^2}{24}, \\ \Pi_{P55} &= \Pi_{P11}, \\ \Pi_{C11} &= \Pi_{P11}, \\ \Pi_{C22} &= \Pi_{P22}.\end{aligned}\tag{A6}$$

The corrected thermal mass of the longitudinally polarized W boson is

$$\bar{M}_{W_L^\pm}^2 = \frac{1}{4}g^2(h_1^2 + h_2^2 + h_3^2) + 2g^2T^2.\tag{A7}$$

The corrected thermal mass of the longitudinally polarized Z and γ boson

$$\bar{M}_{Z_L, \gamma_L}^2 = \frac{1}{8} (g^2 + g'^2) (h_1^2 + h_2^2 + h_3^2) + (g^2 + g'^2) T^2 \pm \Delta, \quad (\text{A8})$$

with

$$\Delta^2 = \frac{1}{64} (g^2 + g'^2)^2 (h_1^2 + h_2^2 + h_3^2 + 8T^2)^2 - g^2 g'^2 T^2 (h_1^2 + h_2^2 + h_3^2 + 4T^2). \quad (\text{A9})$$

[1] C. L. Bennett *et al.* [WMAP], *Astrophys. J. Suppl.* **208**, 20 (2013), arXiv:1212.5225 [astro-ph.CO].

[2] A. D. Sakharov, *Pisma Zh. Eksp. Teor. Fiz.* **5**, 32-35 (1967),

[3] M. Yoshimura, *Phys. Rev. Lett.* **41**, 281-284 (1978).

[4] S. Weinberg, *Phys. Rev. Lett.* **42**, 850-853 (1979).

[5] I. Affleck and M. Dine, *Nucl. Phys. B* **249**, 361-380 (1985).

[6] V. A. Kuzmin, V. A. Rubakov and M. E. Shaposhnikov, *Phys. Lett. B* **155**, 36 (1985).

[7] V. A. Rubakov and M. E. Shaposhnikov, *Usp. Fiz. Nauk* **166**, 493-537 (1996), arXiv:hep-ph/9603208 [hep-ph].

[8] M. Fukugita and T. Yanagida, *Phys. Lett. B* **174**, 45-47 (1986).

[9] M. Trodden, *Rev. Mod. Phys.* **71**, 1463-1500 (1999), arXiv:hep-ph/9803479 [hep-ph].

[10] D. E. Morrissey and M. J. Ramsey-Musolf, *New J. Phys.* **14**, 125003 (2012), arXiv:1206.2942 [hep-ph].

[11] K. Kajantie, M. Laine, K. Rummukainen and M. E. Shaposhnikov, *Phys. Rev. Lett.* **77**, 2887-2890 (1996), arXiv:hep-ph/9605288 [hep-ph].

[12] F. Csikor, Z. Fodor and J. Heitger, *Phys. Rev. Lett.* **82**, 21-24 (1999), arXiv:hep-ph/9809291 [hep-ph].

[13] P. Huet and E. Sather, *Phys. Rev. D* **51**, 379-394 (1995), arXiv:hep-ph/9404302 [hep-ph].

[14] J. McDonald, *Phys. Lett. B* **323**, 339-346 (1994).

[15] J. McDonald, *Phys. Lett. B* **357**, 19-28 (1995).

[16] G. C. Branco, D. Delepine, D. Emmanuel-Costa and F. R. Gonzalez, *Phys. Lett. B* **442**, 229-237 (1998), arXiv:hep-ph/9805302 [hep-ph].

[17] S. Profumo, M. J. Ramsey-Musolf and G. Shaughnessy, *JHEP* **08**, 010 (2007), arXiv:0705.2425 [hep-ph].

[18] V. Barger, P. Langacker, M. McCaskey, M. Ramsey-Musolf and G. Shaughnessy, Phys. Rev. D **79**, 015018 (2009), arXiv:0811.0393 [hep-ph].

[19] M. Jiang, L. Bian, W. Huang and J. Shu, Phys. Rev. D **93**, 065032 (2016), arXiv:1502.07574 [hep-ph].

[20] C. W. Chiang, M. J. Ramsey-Musolf and E. Senaha, Phys. Rev. D **97**, 015005 (2018), arXiv:1707.09960 [hep-ph].

[21] F. P. Huang, Z. Qian and M. Zhang, Phys. Rev. D **98**, 015014 (2018), arXiv:1804.06813 [hep-ph].

[22] K. P. Xie, JHEP **02**, 090 (2021), arXiv:2011.04821 [hep-ph].

[23] W. Chao, Phys. Lett. B **796**, 102-106 (2019), arXiv:1706.01041 [hep-ph].

[24] B. Grzadkowski and D. Huang, JHEP **08**, 135 (2018), arXiv:1807.06987 [hep-ph].

[25] Y. Xiao, J. M. Yang and Y. Zhang, JHEP **02**, 008 (2023), arXiv:2207.14519 [hep-ph].

[26] Y. Xiao, J. M. Yang and Y. Zhang, Sci. Bull. **68**, 3158-3164 (2023), arXiv:2307.01072 [hep-ph].

[27] C. Balázs, Y. Xiao, J. M. Yang and Y. Zhang, Nucl. Phys. B **1002**, 116533 (2024), arXiv:2301.09283 [hep-ph].

[28] N. Turok and J. Zadrozny, Nucl. Phys. B **358**, 471-493 (1991).

[29] J. M. Cline, K. Kainulainen and A. P. Vischer, Phys. Rev. D **54**, 2451-2472 (1996), arXiv:hep-ph/9506284 [hep-ph].

[30] L. Fromme, S. J. Huber and M. Seniuch, JHEP **11**, 038 (2006), arXiv:hep-ph/0605242 [hep-ph].

[31] J. M. Cline, K. Kainulainen and M. Trott, JHEP **11**, 089 (2011), arXiv:1107.3559 [hep-ph].

[32] S. Tulin and P. Winslow, Phys. Rev. D **84**, 034013 (2011), arXiv:1105.2848 [hep-ph].

[33] T. Liu, M. J. Ramsey-Musolf and J. Shu, Phys. Rev. Lett. **108**, 221301 (2012), arXiv:1109.4145 [hep-ph].

[34] M. Ahmadvand, Int. J. Mod. Phys. A **29**, 1450090 (2014), arXiv:1308.3767 [hep-ph].

[35] C. W. Chiang, K. Fuyuto and E. Senaha, Phys. Lett. B **762**, 315-320 (2016), arXiv:1607.07316 [hep-ph].

[36] H. K. Guo, Y. Y. Li, T. Liu, M. Ramsey-Musolf and J. Shu, Phys. Rev. D **96**, 115034 (2017), arXiv:1609.09849 [hep-ph].

[37] D. Goncalves, P. A. N. Machado and J. M. No, Phys. Rev. D **95**, 055027 (2017), arXiv:1611.04593 [hep-ph].

[38] K. Fuyuto, W. S. Hou and E. Senaha, Phys. Lett. B **776**, 402-406 (2018), arXiv:1705.05034 [hep-ph].

[39] T. Modak and E. Senaha, Phys. Rev. D **99**, 115022 (2019), arXiv:1811.08088 [hep-ph].

[40] P. Basler, L. Biermann, M. Mühlleitner and J. Müller, Eur. Phys. J. C **83**, 57 (2023), arXiv:2108.03580 [hep-ph].

[41] P. Basler, M. Mühlleitner and J. Müller, Comput. Phys. Commun. **269**, 108124 (2021), arXiv:2007.01725 [hep-ph].

[42] R. Zhou and L. Bian, Phys. Lett. B **829**, 137105 (2022), arXiv:2001.01237 [hep-ph].

[43] K. Enomoto, S. Kanemura and Y. Mura, JHEP **01**, 104 (2022), arXiv:2111.13079 [hep-ph].

[44] D. Gonçalves, A. Kaladharan and Y. Wu, Phys. Rev. D **105**, 095041 (2022) arXiv:2108.05356 [hep-ph].

[45] K. Enomoto, S. Kanemura and Y. Mura, JHEP **09**, 121 (2022), arXiv:2207.00060 [hep-ph].

[46] G. Arcadi, N. Benincasa, A. Djouadi and K. Kannike, Phys. Rev. D **108**, 055010 (2023), arXiv:2212.14788 [hep-ph].

[47] J. Baron *et al.* [ACME], Science **343**, 269-272 (2014), arXiv:1310.7534 [physics.atom-ph].

[48] S. J. Huber, K. Mimasu and J. M. No, Phys. Rev. D **107**, 075042 (2023), arXiv:2208.10512 [hep-ph].

[49] S. Liu and L. Wang, Phys. Rev. D **107**, 115008 (2023), arXiv:2302.04639 [hep-ph].

[50] J. Ma, J. Wang and L. Wang, Phys. Rev. D **109**, 075024 (2024), arXiv:2311.02828 [hep-ph].

[51] J. Gao, J. Ma, L. Wang and H. Xu, arXiv:2408.03705 [hep-ph].

[52] H. H. Patel and M. J. Ramsey-Musolf, JHEP **07**, 029 (2011), arXiv:1101.4665 [hep-ph].

[53] S. R. Coleman and E. J. Weinberg, Phys. Rev. D **7**, 1888-1910 (1973).

[54] L. Dolan and R. Jackiw, Phys. Rev. D **9**, 3320-3341 (1974).

[55] P. Athron, C. Balázs, A. Fowlie, L. Morris and L. Wu, Prog. Part. Nucl. Phys. **135**, 104094 (2024), arXiv:2305.02357 [hep-ph].

[56] S. L. Glashow and S. Weinberg, Phys. Rev. D **15**, 1958 (1977).

[57] A. Pich and P. Tuzon, Phys. Rev. D **80**, 091702 (2009), arXiv:0908.1554 [hep-ph].

[58] A. Beniwal, M. Lewicki, M. White and A. G. Williams, JHEP **02**, 183 (2019), arXiv:1810.02380 [hep-ph].

[59] D. A. Kirzhnits and A. D. Linde, Annals Phys. **101**, 195-238 (1976).

[60] C. W. Chiang, Y. T. Li and E. Senaha, Phys. Lett. B **789**, 154-159 (2019), arXiv:1808.01098

[hep-ph].

- [61] P. Athron, C. Balazs, A. Fowlie, L. Morris, G. White and Y. Zhang, JHEP **01**, 050 (2023), arXiv:2208.01319 [hep-ph].
- [62] R. R. Parwani, Phys. Rev. D **45**, 4695 (1992), arXiv:hep-ph/9204216 [hep-ph].
- [63] P. B. Arnold and O. Espinosa, Phys. Rev. D **47**, 3546 (1993), arXiv:hep-ph/9212235 [hep-ph].
- [64] A. Drozd, B. Grzadkowski, J. F. Gunion and Y. Jiang, JHEP **11**, 105 (2014), arXiv:1408.2106 [hep-ph].
- [65] X. G. He and J. Tandean, JHEP **12**, 074 (2016), arXiv:1609.03551 [hep-ph].
- [66] H. J. He, N. Polonsky and S. f. Su, Phys. Rev. D **64**, 053004 (2001), arXiv:hep-ph/0102144 [hep-ph].
- [67] H. E. Haber and D. O’Neil, Phys. Rev. D **83**, 055017 (2011), arXiv:1011.6188 [hep-ph].
- [68] P. A. Zyla *et al.* [Particle Data Group], PTEP **2020**, 083C01 (2020).
- [69] P. Athron, C. Balázs, A. Fowlie and Y. Zhang, Eur. Phys. J. C **80**, 567 (2020), arXiv:2003.02859 [hep-ph].
- [70] A. Ahriche, Phys. Rev. D **75**, 083522 (2007), arXiv:hep-ph/0701192 [hep-ph].
- [71] A. Ahriche, T. A. Chowdhury and S. Nasri, JHEP **11**, 096 (2014), arXiv:1409.4086 [hep-ph].
- [72] M. Hindmarsh, S. J. Huber, K. Rummukainen and D. J. Weir, Phys. Rev. D **92**, 123009 (2015), arXiv:1504.03291 [astro-ph.CO].
- [73] J. M. No, Phys. Rev. D **84**, 124025 (2011), arXiv:1103.2159 [hep-ph].
- [74] J. R. Espinosa, T. Konstandin, J. M. No and G. Servant, JCAP **06**, 028 (2010), arXiv:1004.4187 [hep-ph].
- [75] H. K. Guo, K. Sinha, D. Vagie and G. White, JCAP **01**, 001 (2021), arXiv:2007.08537 [hep-ph].
- [76] J. Ellis, M. Lewicki and J. M. No, JCAP **07**, 050 (2020), arXiv:2003.07360 [hep-ph].
- [77] X. Wang, F. P. Huang and X. Zhang, JCAP **05**, 045 (2020), arXiv:2003.08892 [hep-ph].
- [78] C. Caprini, R. Durrer and G. Servant, JCAP **12**, 024 (2009), arXiv:0909.0622 [astro-ph.CO].
- [79] P. Binetruy, A. Bohe, C. Caprini and J. F. Dufaux, JCAP **06**, 027 (2012), arXiv:1201.0983 [gr-qc].
- [80] M. B. Hindmarsh, M. Lüben, J. Lumma and M. Pauly, SciPost Phys. Lect. Notes **24**, 1 (2021), arXiv:2008.09136 [astro-ph.CO].
- [81] A. D. Linde, Phys. Lett. B **100**, 37-40 (1981).
- [82] C. L. Wainwright, Comput. Phys. Commun. **183**, 2006-2013 (2012), arXiv:1109.4189 [hep-ph].

- [83] P. Amaro-Seoane *et al.* [LISA], arXiv:1702.00786 [astro-ph.IM].
- [84] X. Gong, Y. K. Lau, S. Xu, P. Amaro-Seoane, S. Bai, X. Bian, Z. Cao, G. Chen, X. Chen and Y. Ding, *et al.* J. Phys. Conf. Ser. **610**, 012011 (2015), arXiv:1410.7296 [gr-qc].
- [85] J. Luo *et al.* [TianQin], Class. Quant. Grav. **33**, 035010 (2016), arXiv:1512.02076 [astro-ph.IM].
- [86] K. Yagi and N. Seto, Phys. Rev. D **83**, 044011 (2011), arXiv:1101.3940 [astro-ph.CO].
- [87] H. Kudoh, A. Taruya, T. Hiramatsu and Y. Himemoto, Phys. Rev. D **73**, 064006 (2006), arXiv:gr-qc/0511145 [gr-qc].